Applied Catalysis B: Environmental 181 (2016) 727–737

Contents lists available at ScienceDirect

Applied Catalysis B: Environmental

journal homepage: www.elsevier.com/locate/apcatb

Optimization of the preparation method of CuO/CeO_2 structured catalytic monolith for CO preferential oxidation in H_2-rich streams

Gianluca Landi[a], Paola Sabrina Barbato[a,*], Almerinda Di Benedetto[b], Luciana Lisi[a]

[a] Research Institute on Combustion-CNR, Naples, Italy
[b] Department of Chemical, Materials and Industrial Production Engineering, Univ. of Naples Federico II, Naples, Italy

ARTICLE INFO

Article history:
Received 28 May 2015
Received in revised form 22 August 2015
Accepted 24 August 2015
Available online 28 August 2015

Keywords:
CO-PROX
Monolith
CuO/CeO_2
Adhesion
Slurry preparation

ABSTRACT

Copper/ceria washcoated monoliths were prepared by a modified dip coating procedure and operated under CO-PROX conditions. Slurry preparation was suitably modified with respect to more conventional procedure in order to improve the washcoat adhesion onto the cordierite walls. Wet instead of dry milling of the powder ceria used to prepare slurry and colloidal ceria addition to the slurry significantly improved washcoat adhesion, due to partial penetration of the washcoat into the cordierite macropores. Moreover, ceria specific surface area and pore size distribution were affected by both preparation and composition of slurry. Samples prepared by modified slurries showed also improved copper dispersion with a consequent higher selectivity to CO_2.

1. Introduction

Carbon monoxide preferential oxidation has been widely studied as a possible purification step of hydrogen rich stream for PEM fuel cell applications, requiring less than 50 ppm CO [1,2].

The main interest for PEMFC is related to small scale power generation, requiring low pressure drops, compact catalytic reactor and robustness. Packed-bed reactors cannot fulfill the above requirements [3,4] and need a proper design, including heat exchange with the reacting flow in order to get an optimal reaction temperature [5]. On the contrary, catalytic monoliths appear the best choice for CO-PROX application. The interest towards monolithic reactors for CO-PROX is recent and quite limited [4,6–13].

Copper/ceria catalyst has been proposed as an alternative to noble metal catalysts due to its activity and selectivity at low temperatures for CO-PROX reaction [14–21].

In previous papers, Cu/CeO_2 washcoated structured systems have been prepared and tested as CO-PROX catalysts [4,6,9,22]. A relevant issue in the preparation of monolithic catalysts is the adhesion stability of the washcoat. However, conventional methods for the deposition of catalysts on metallic or ceramic substrates, such as impregnation and dip-coating, do not ensure a suitable adhesion. Zeng et al. [6] used sol-pyrolysis technique for depositing $CuO–CeO_2$ on FeCrAl honeycomb supports finding good adhesion stability in ultrasonic and thermal shock tests.

Gu et al. [4] used three different methods to deposit CuO/CeO_2 onto meso-macroporous alumina substrates: citrate, urea combustion and impregnation method. They found that catalysts with CuO/CeO_2 loaded by the citrate method show the best catalytic performance maintaining the structural characteristics of active CuO/CeO_2 powder catalysts, including high dispersion of copper species, nanometer ceria particle size and strong interaction between copper and ceria.

Nevertheless, we recently prepared CuO/CeO_2 based catalysts by conventional dip-coating of honeycomb cordierite monoliths which provided a limited washcoat adhesion [13].

In this work we aim at improving washcoat adhesion on the substrate walls by modifying the slurry used during structured catalysts preparation. To this end we prepared monolithic reactors by changing type and time of ceria milling and the colloidal ceria amount. All the samples were tested toward the adhesion and the CO-PROX performances.

2. Experimental

2.1. Catalyst preparation

We previously reported the technique for monolith preparation [13]. Briefly, commercial honeycomb monoliths (cordierite, 400 cpsi; Corning) were cut in the desired shape and dimension

* Corresponding author. Fax: +39 0815936936.
E-mail address: barbato@irc.cnr.it (P.S. Barbato).

http://dx.doi.org/10.1016/j.apcatb.2015.08.040
0926-3373/

(cylinder; $D = 16$ mm; $L = 12$ mm) and then washcoated with a ceria (SSA = 56 m^2/g, Grace) layer by modified dip coating procedure. Subsequently monoliths were dried at 120 °C for 1 h and calcined in air at 450 °C for 2 h. This procedure was repeated until the desired ceria weight deposited on the monolith walls was obtained which, according to the supposed ceria density, should correspond to about 15 μm layer. Copper oxide was deposited onto ceria by wet impregnation using an aqueous solution of copper acetate monohydrate (Sigma–Aldrich); the samples were then dried at 120 °C for 1 h and calcined in air at 450 °C for 2 h in order to obtain copper oxide. The procedure was repeated until the desired copper oxide load was obtained (4.2 wt.% with respect to the active layer).

In our previous work [13] we prepared ceria washcoated monolith showing good catalytic performance in CO-PROX but an inadequate adhesion of the washcoat layer. In this work, we aim at improving the adhesion by modifying the particle size distribution of the ceria powder used to prepare the slurry.

First we changed the milling procedure of the starting CeO_2 powder. Milling was performed in a planetary ball mill (Retsch PM 100). Particle size distribution was measured by means of a Malvern Mastersizer 2000 Hydro 2000 S laser diffraction particle size analyzer. Ceria powder was milled under dry condition for a time ranging from 5 to 30 min. Some samples were prepared by wet milling for 30–60 min adding bi-distilled water as dispersing medium.

Other samples were prepared adding colloidal ceria (Nyacol Nano Technologies Inc., CeO_2 particle size <20 nm) to CeO_2 powder; moreover, in order to address the effect of colloidal ceria we also prepared a monolith using a slurry containing colloidal ceria only. The volume of colloidal suspension added to the slurry was chosen taking into account that 100 ml colloidal ceria suspension contains 24.4 g ceria thus keeping constant the total amount of ceria in the washcoat. Finally, we prepared a monolith using a 4.2 wt.% CuO on CeO_2 catalyst as powder to prepare the slurry. The powder catalyst was obtained by wet impregnation according to [17] and then wet milled before slurry preparation. This catalyst was also used as reference for the reaction tests.

Hereafter, monoliths will be labelled as *Sx-M*, where *Sx* indicate the slurry used to coat the monolithic substrate *M*.

2.2. Physico-chemical characterization

2.2.1. Powders

A fraction of slurries used for washcoating monoliths was dried and calcined for 2 h at 450 °C in order to obtain powders with the same nature of the corresponding washcoat to be characterised. Specific surface area (SSA) and porosity were determined by N_2 adsorption at 77 K using a Quantachrome Autosorb-1C instrument after degassing samples at 150 °C for 1.5 h.

2.2.2. Monoliths

The actual metal content was measured by means of ICP-MS analysis (Agilent 7500CE instrument). A FEY Inspect-S instrument was used to record SEM images. Monoliths were cut in order to analyze inner channels.

In order to test the adhesion of the washcoat on the cordierite walls, dried monoliths were placed in an ultrasound bath for 15 min and the weight loss was measured. The weight loss percentage was related to the ceria washcoat and calculated according to the following equation

$$\frac{W_f - W_u}{W_f - W_0} \times 100$$

where W_f is the monolith weight at the end of the washcoating procedure, W_u is the monolith weight after sonication and W_0 is the weight of the uncoated monolith.

Reducibility of structured catalysts was studied by Temperature Programmed Reduction (TPR) analysis carried out in a quartz reactor using a 2 vol.% H_2/N_2 mixture with a contact time of 0.077 g s/cm^3. The samples were previously oxidized with 10 vol.% O_2 at 450 °C and then purged with N_2 at room temperature. During all TPR tests the reactor was heated at 10 °C/min up to 450 °C, maintaining the temperature for 1 h. Hydrogen uptake was monitored using a Fisher-Rosemount NGA2000 continuous analyzer. Due to the possible water vapor interference with the analysis of hydrogen, H_2O was separated from the gas mixture upstream of the analyzer by a $CaCl_2$ trap. TPR profiles were fitted by a Fityk software (free version 0.9.1) [23] in order to separate different contributions to the overall reduction profile.

2.3. Catalytic tests

The lab-scale set-up used for CO-PROX experiments and the reactor set-up are described elsewhere [13,24]. A tubular quartz reactor was used to hold the monoliths, while two mullite foams located upstream and downstream acted as flow equalizers. A ceramic wool tape was used to wrap both monolith and foams. Before the catalytic tests, monoliths were sonicated to remove the fraction of washcoat not anchored to the substrate walls. As a consequence, they are not expected to lose further weight during the catalytic tests. The contact times are calculated on the basis of the weight of sonicated monoliths.

The temperature profiles were measured by means of three thermocouples placed inside the central channel of the monolith as described in [13]. An electric tubular furnace (Lenton) provided with a PID-type controller was used to pre-heat the catalytic reactor. The reacted flow was dried by means of an ice bath based condenser and a $CaCl_2$ trap and then sent to a Fisher-Rosemount NGA2000 continuous analyzer in order to continuously monitor CO, CO_2, H_2 and O_2 concentrations.

Catalytic tests were run at fixed contact time, $\tau = 0.054\ g_{cat}$ s/ml(STP), g_{cat} being the catalyst weight, cordierite substrate excluded. The reactants concentrations were fixed at 50 vol.%, 0.5 vol.% and 0.9 vol.% for hydrogen, carbon monoxide and oxygen respectively, nitrogen as balance. Reaction temperature was set between 80 and 200 °C. Mass balance was always closed within ± 4%. Reactants conversions and selectivity of oxygen reacting with carbon monoxide were calculated according to the following equations:

$$x_{CO} = \frac{CO^{IN} - CO^{OUT}}{CO^{IN}} \quad x_{O_2} = \frac{O_2^{IN} - O_2^{OUT}}{O_2^{IN}}$$

$$x_{H_2} = \frac{H_2^{IN} - H_2^{OUT}}{H_2^{IN}} \quad s_{CO} = \frac{\Delta O_2^{CO}}{\Delta O_2^{CO} + \Delta O_2^{H_2}} = 0.5 \cdot \frac{CO^{IN} - CO^{OUT}}{O_2^{IN} - O_2^{OUT}}$$

where xCO, xO$_2$, xH$_2$ and sCO are, respectively, the CO, O_2 and H_2 conversions and the O_2 selectivity to CO_2 and $\Delta O_2{}^{CO}$ and $\Delta O_2{}^{H2}$ the oxygen moles consumed for CO and H_2 oxidation respectively.

3. Results

3.1. Preliminary results on powder particle size distribution

Ceria powder was milled under both dry and wet conditions. In Fig. 1a the effect of milling time under dry condition on the particle size distribution is shown. According to Ayastuy et al. [9], a good adhesion can be obtained starting from a powder with 1–3 μm particles. By increasing the milling time the particle distribution broadens and the fractions below 1 μm and above 10 μm increase, suggesting that a longer milling causes not only the expected

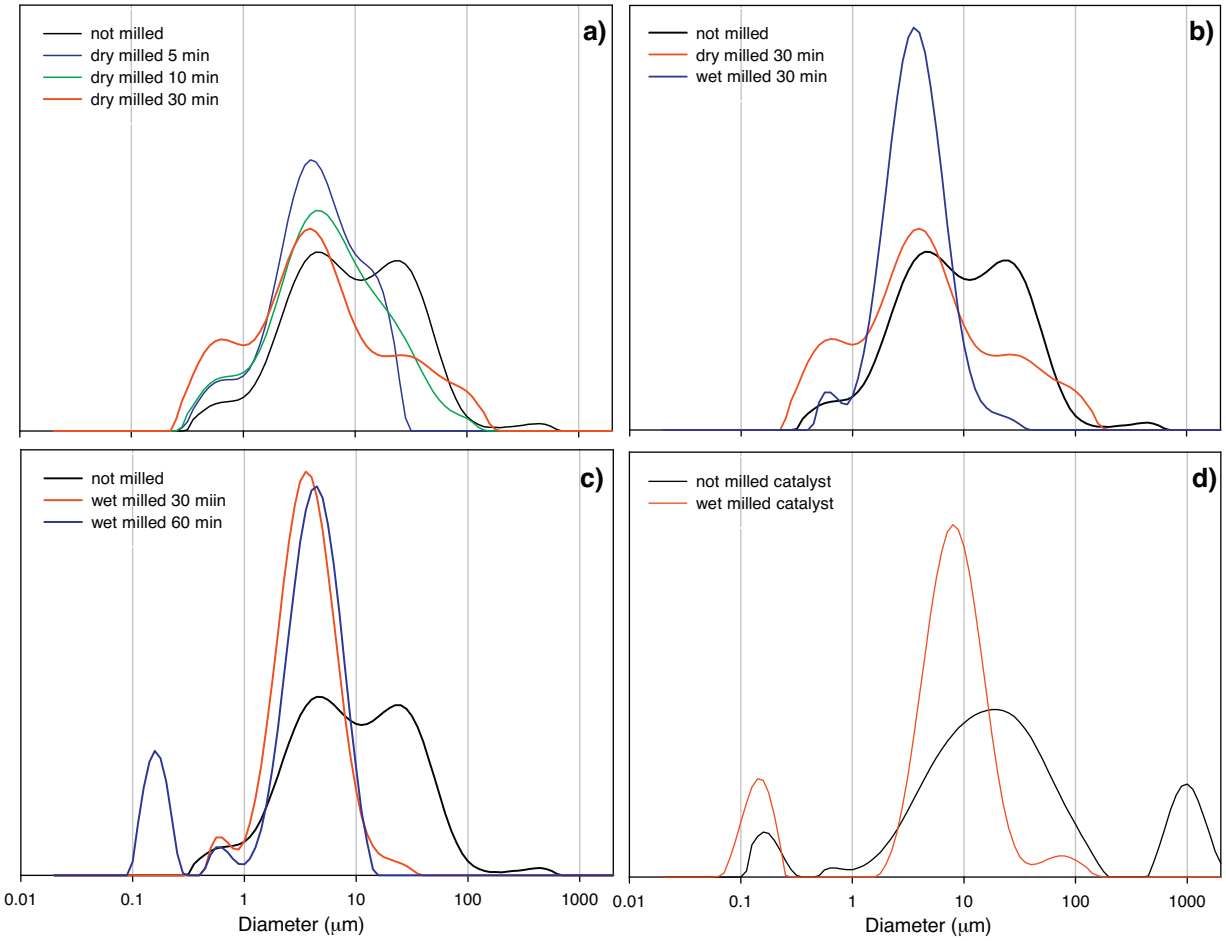

Fig. 1. Particle size distribution obtained by dry (a) and wet (c) milling of ceria. Comparison of particle size distribution obtained by dry and wet milling performed for 30 min (b). Particle size distribution of as prepared and wet milled 4.2 wt.% CuO/CeO_2 catalyst (d).

formation of finer particles but also the aggregation of 1–10 μm particles. Accordingly, slurry S1 was prepared limiting the milling time to 5 min. Slurry S1 was used to prepare monoliths reported in [13].

A larger fraction of 1–10 μm particles can be obtained by wet milling, using bi-distilled water as dispersing medium (Fig. 1b). Nevertheless, a very long wet milling causes the formation of ultrafine particles giving a bi-modal distribution with an additional peak centered at 0.2 μm (Fig. 1c). In order to avoid these ultrafine particles, slurry S2 was prepared with a ceria milled for 30 min. Slurry S6, containing copper/ceria catalyst instead of ceria, was prepared with a wet milled powder; milling time was set to 30 min, as for slurry S2. The corresponding particle size distribution is reported in Fig. 1d. In this case, the starting powder contains a fraction below 1 μm, slightly increased after milling procedure.

Slurries S3 and S4 were prepared by partially substituting the ceria provided by Grace with colloidal ceria (Nyacol Nano Technologies Inc.) keeping constant the total CeO_2 amount. As a consequence, the volume of colloidal suspension was chosen taking into account that 100 ml colloidal ceria suspension contains 24.4 g ceria.

In Table 1 the compositions of the different slurries are summarized.

3.2. Slurry characterization

Specific surface are (SSA) and pore volume of the calcined slurries are given in Table 2. SSA slightly increases by wet milling due to a larger fraction of smaller particles. On the other hand, the very small particle size (about 20 nm) of colloidal ceria is the reason of the increasing SSA of slurries obtained by adding different amounts of the colloidal suspension. The increase of SSA is roughly proportional to the fraction of colloidal ceria up to 75%, the S4 sample showing a SSA close to that of the slurry prepared using only colloidal ceria (S5).

In Fig. 2 the N_2 adsorption/desorption isotherms of the different slurries are shown. The curves can be divided into two groups: (i) S1, S2, S3 and S6 which, except for the presence of a very small fraction of micropores (steep increase of adsorbed N_2 volumes at very low p/p^0), show the typical isotherm of mesoporous materials with the hysteresis between adsorption and desorption branches (ii) S4 and S5 showing the characteristic isotherm of microporous materials with the initial steep increase and the almost flat zone at intermediate p/p^0.

Evaluation of pore size distribution (PSD) according to the BJH model was first attempted but this model, which does not provide a good evaluation of the micropores filling, failed for S4 and S5. As a consequence, a DFT treatment was used which give a more accurate approach for micropore analysis [25]. The best fitting was found for all samples using a slit pore equilibrium model. In Fig. 3 the PSD of the slurries evaluated according to this model is shown. S1, S2 and S6 have mostly mesopores peaked at about 40 Å, the wet milling providing a slightly greater fraction of these pores. The addition of colloidal ceria is associated to the appearance of micropores centered at 15 Å and to the reduction of the mesopores amount. The total pore volume is affected by the slurry composi-

Table 1
Compositions of the slurries.

Slurry	Composition					
	H_2O, ml	HNO_3 (65 wt.%), g	CeO_2 (Grace), g	Milling time,min	Nyacol® colloidal ceria, ml	4.2 wt.% CuO/CeO_2, g
S1	100	2.16	25.0	5	–	–
S2[a]	100	2.16	25.0	30	–	–
S3	50	1.08	12.5	5	50	–
S4	25	0.54	6.25	5	75	–
S5	–	–	–	–	100	–
S6[a]	100	2.16	–	30	–	25

[a]Wet milling.

Table 2
Surface area and pore volume of the slurries.

Slurry	SSA (BET), m^2/g	Micro-pore volume, cm^3/g	Total pore volume, cm^3/g	Micro/Meso pores ratio
S1	59	0.0036	0.12	0.031
S2	67	0.0033	0.13	0.026
S3	90	0.011	0.11	0.11
S4	112	0.024	0.083	0.41
S5	119	0.031	0.077	0.67
S6	72	0.0064	0.12	0.053

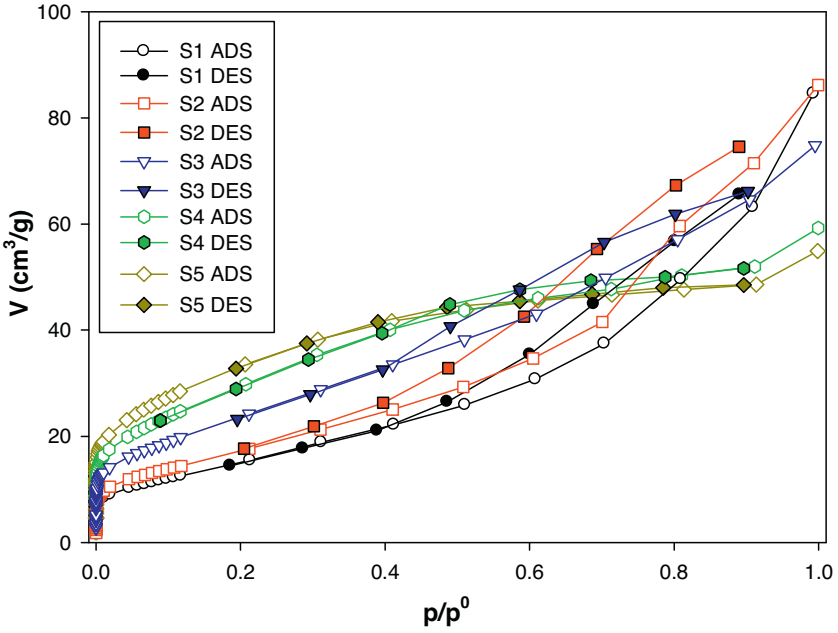

Fig. 2. Adsorption and desorption isotherms of different slurries.

tion as well (Table 2). Slurries with a dominance of mesopores have higher values of total pore volume. On the contrary, slurries with 75 and 100% colloidal ceria have a lower total pore volume which is mostly related to the micropores contribution. In agreement, ratio between meso and micropores decreases by increasing the fraction of colloidal ceria in the slurry as reported in Table 2.

Due to the very similar porous structure of S4 and S5 slurries, S4 slurry was not further investigated and S5 was chosen as representative of the microporous materials containing colloidal ceria.

3.3. Monoliths characterization

In Table 3 the weight loss of ceria washcoat after monoliths sonication is reported for the different slurries. With respect to S1-M monolith, used as reference [13], the other monoliths show a very good adhesion, independently of the slurry composition, ceria loss being negligible for S2-M to S6-M. The main difference between slurry S1 and the other suspensions is the particle size distribution, discussed in the paragraph 3.1 which suggests that the large fraction of particle in the range 10–100 μm of the starting ceria powder (the one used for S1) inhibits the adhesion of the washcoat layer. On the other hand, cordierite is characterized by its own porosity, including both meso- and macropores.

Table 3
Ceria weight loss, theoretical (after sonication) and measured thickness of washcoats on monoliths prepared by different slurries.

Monolith	Ceria loss, %	h_t, μm	h_m μm
S1-M	17	17	14–15
S2-M	0.1	15	9–10
S3-M	1.3	18	8–10
S5-M	0.3	14	<5
S6-M	0.3	14	9–10

The sponge-like structure of cordierite is shown in Fig. 4. When a sol is used for coating the walls of a cordierite honeycomb, it

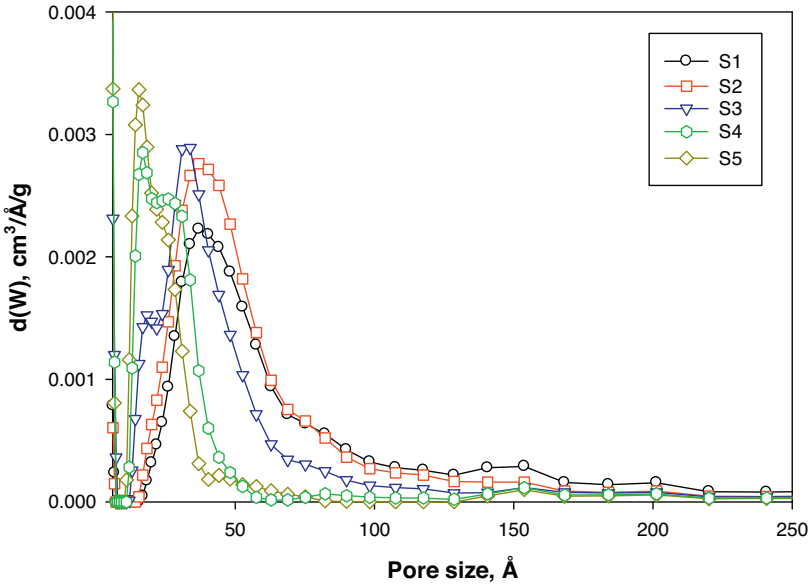

Fig. 3. PSD of different slurries evaluated according to slit pore model (DFT method).

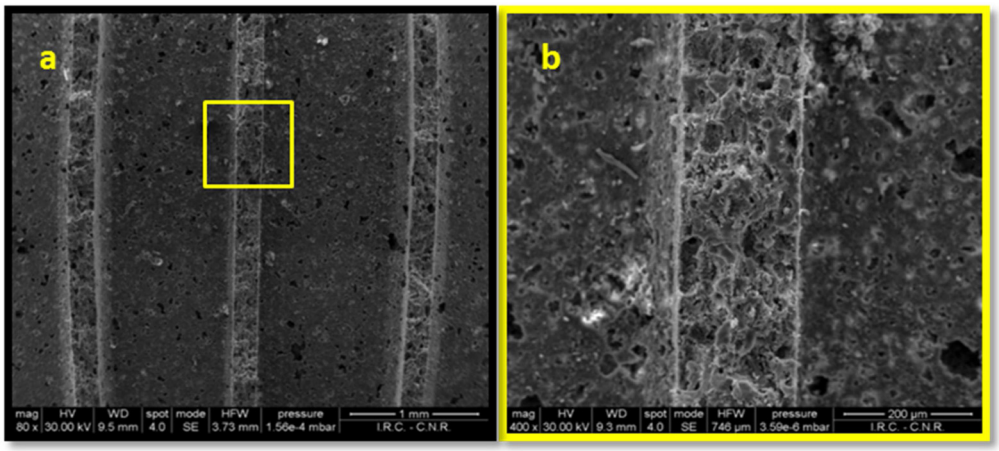

Fig. 4. SEM images of cordierite substrate. Images b is magnification of the yellow-framed area.

can very easily penetrate and gel into the honeycomb pores, thus leading to "waste" material [26], namely to washcoat not easily accessible by gaseous reactants. This behavior can be extended to slurries containing particles with characteristic dimensions lower or comparable to those of the cordierite pores. In Table 3 the theoretical thickness of the washcoat layers after sonication (h_t), i.e. estimated on the basis of the washcoat weight after sonication and its apparent density, is reported and compared to those measured by SEM analysis (h_m). h_t values are higher than the h_m values for all the samples. This can be explained by ceria accumulation in the corners of the channels, as it generally occurs in the monoliths. Nevertheless, the larger difference between h_t and h_m detected for monoliths prepared with slurries S2-S6 suggests that a part of the ceria washcoat penetrated into the cordierite pores.

A deeper penetration of ceria into the monolith walls can be noted in the SEM image of S2-M and S3-M and compared to the corresponding one of S1-Mreported in Fig. 5 (yellow frames). A more dense material filling the large pores of the substrate is visible in the SEM image of the monoliths cross section of S2-M and S3-M. Another sign of washcoat penetration into cordierite is the feature of the washcoat surface in the channel still showing some of the large holes of the substrate in the SEM images of S2-M and S3-M(Fig. 5, black frames), not appearing on S1-M which shows a quite compact and uniform surface. When only nanometric ceria is used for the washcoat (slurry S5), this phenomenon is even more evident, sponge-like structure of the original cordierite substrate appearing almost unaltered. Thus, for monoliths with the strongest adhesion of the washcoat the ceria layer is well anchored to the surface fitting holes and keeping the original roughness of cordierite. Accordingly, the surface appearance of the washcoat layers is different (Fig. 5, red frames). The S1-M monolith is characterized by a washcoat mainly constituted by the agglomeration of particles with a mean size of few microns. By increasing the number of ultrafine particles (by wet milling (S2-M) or by colloidal ceria addition (S3-M)), the particles characteristic of S1-M monolith still appear, but are inserted in a more uniform and compact matrix. Finally, the washcoat of S5-M monolith consists only of a compact layer mostly cracked due to the drying thermal treatment. SEM images

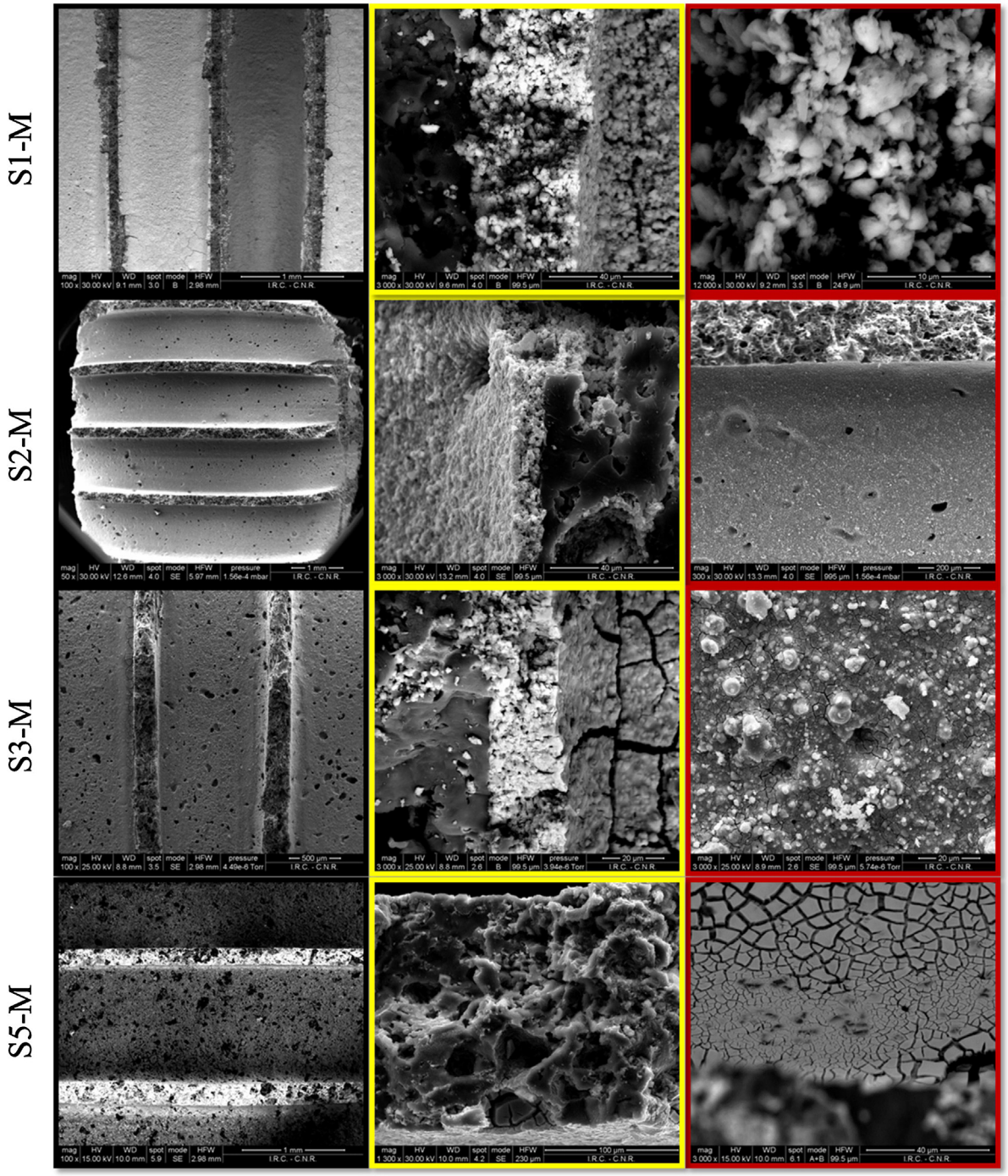

Fig. 5. SEM images of monoliths. Cross sections of walls and washcoats are yellow-framed; images of channel surface are red-framed. (For interpretation of the references to colour in this figure legend and in the text, the reader is referred to the web version of this article.)

of S6-M are similar to those of S2-M, due to the same preparation method of the corresponding slurries and, thus, are not reported. An even more evident sign of the washcoat penetration into the cordierite walls is shown in Fig. 6 showing the Ce distribution into the interior of the substrate wall, compared to that of S1-M. In contrast with what observed for S1-M [13], Ce was rather uniformly detected into wall. The same element was found mainly located on the surface of the cordierite for S1-M.

ICP-MS analysis of the final monoliths (i.e. after copper deposition) revealed that copper content is very close to the nominal one, except for S6-M monolith which has a copper content (2.75 wt.%) lower than the theoretical value (4.2 wt.%). Cu loss corresponds to about 35% and it is due to Cu leaching in the S6 suspension, related to its acid pH [27].

3.4. H_2-TPR on monoliths

In Fig. 7 H_2-TPR profiles of structured catalysts are reported, showing the effect of the slurry preparation on the CuO/CeO_2 reducibility under hydrogen flow. It is worth noting that peak positions, as reported in Fig. 7, are those corresponding to the signal deconvolution, as stated in par. 2.2. This means that, due to the overlapping of different peaks, peak maxima do not exactly correspond to TPR maxima. In Table 4 the H_2 consumptions and H_2/Cu

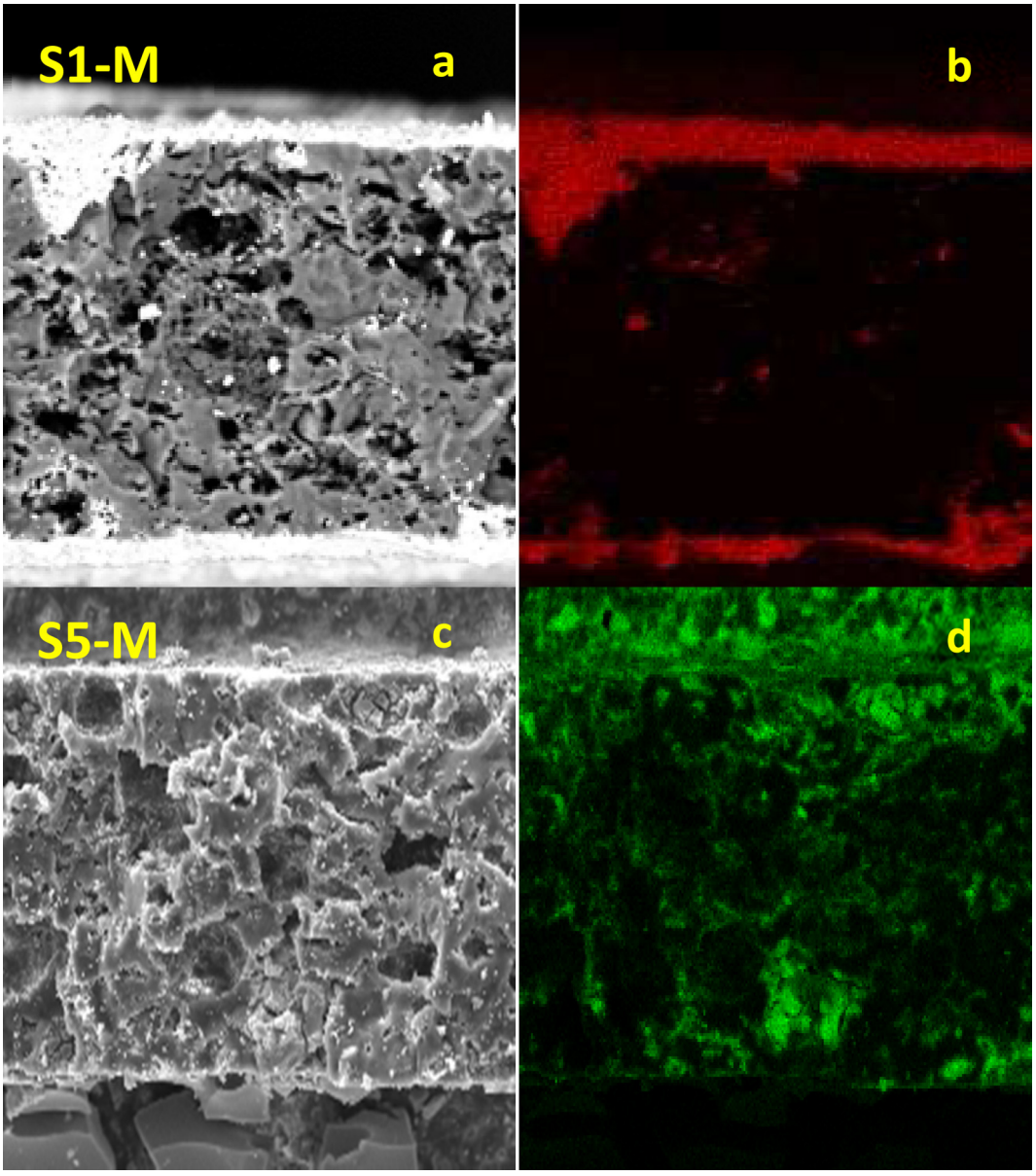

Fig. 6. SEM images (a, c) and corresponding EDS maps reporting Ce distribution (b, d) of an interior of the substrate wall of the S1-M (a, b) and S5-M (c, d). (For interpretation of the references to colour in this figure legend, the reader is referred to the web version of this article.)

Table 4
H_2 consumptions and H_2/Cu ratios measured during H_2-TPR of powder and structured CuO/CeO_2 catalysts.

	H_2 consumption, (μmol/g)	H_2/Cu
Powder	786	1.5
S1-M	1050 (980[a])	1.8[a]
S2-M	865	1.6
S3-M	988	1.9
S5-M	1110	2.2
S6-M	636	1.8

[a] Excluding δ peak.

ratios are reported. Except for S5-M, the TPR profiles show three main peaks (α, β and γ) which are found also for the TPR curves of the powder catalyst [28]. The intermediate peak is not evident for S5-M due to the strong dominance of the signals at lower and higher temperature. Moreover, an additional peak at very high temperature (δ) is present only for S1-M which can be addressed to copper oxide not in contact with ceria. Unsupported CuO was found in the cordierite macropores due to the bad coating of the substrate, as shown by SEM images [13]. It has been reported that the reduction of CuO aggregates occurs at lower temperatures [29], however, unsupported CuO in S1-M is located in less accessible void volumes of cordierite, thus explaining the shift of the reduction peak towards higher temperatures.

On the other monolith samples the good coating of cordierite surface and ceria penetration into the cordierite macropores result in an effective contact between copper and ceria and, consequently, these samples do not show the high temperature signal. Finally, the strong copper leaching taking place in the S6-M preparation seems to remove, almost uniformly, many reducible species providing a broad signal where it is difficult to distinguish different peaks.

As shown in Table 4, H_2 consumption is higher than that corresponding to complete copper reduction (H_2/Cu = 1), as generally occurring on copper/ceria systems due to the promoting effect of copper-ceria interaction [28,30–31]. The H_2 excess with respect to the stoichiometric value is even higher for the structured catalyst compared to the powder sample suggesting a larger contact

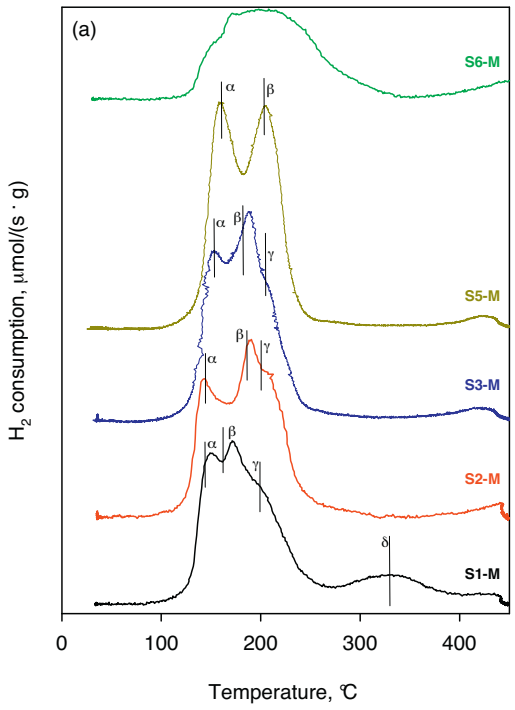

Fig. 7. H_2-TPR profiles of structured CuO/CeO_2 catalysts. Peak positions as obtained by signal deconvolution.

between copper and ceria which is the main reason for ceria reduction at temperatures much lower than those required for pure CeO_2 reduction [28,31].

The α peak is addressed to the reduction of copper species strongly interacting with ceria [28,31] which are mainly CO oxidation sites [24].

β peak may be related to large CuO clusters formed on the ceria surface [28,31] and are responsible for H_2 oxidation [24]. Finally, γ peak can be addressed to surface ceria reduction promoted by copper [21], in agreement with the detection of three sites by CO_2 titration [24].

In Fig. 8 the results of peak fitting of the TPR profiles in terms of peak temperature (a) and H_2 consumption related to different peaks (b) are shown. The peak temperature of each signal increases from S1-M to S5-M (Fig. 8a), i.e. a general shift towards higher temperatures occurs by increasing the surface area of the sample. The most significant increase is related to T_β, while T_γ is almost constant. It is worth noting that T_β for S5-M is very close to T_γ so, the big overlapping of the corresponding peaks suggested to consider β and γ peaks as a single signal in the subsequent correlation reported in Fig. 8b where the total H_2 uptake and the ratio between α and the sum of γand β peaks are reported as a function of SSA. The increase of surface area leads to an increase of the total H_2 consumption which is mainly related to the increase of α peak and to the detriment of β and γ peaks. This suggests that by increasing the surface area copper dispersion is improved and, as a consequence, a larger number of copper species strongly interacting with ceria are formed with a simultaneous reduction of the other copper species. The increase is almost linear if S5-M sample is excluded. S5-M monolith has different features with respect to the other samples, in terms of porosity structure.

It must be pointed out that both copper species strongly interacting with ceria (α peak) and CuO clusters (β peak) appear less reducible by hydrogen, as indicated by the increase of the reduction temperatures, however, the difference between T_α and T_β increases on increasing the surface area with an expected larger difference between the activation temperature of CO oxidation and that of H_2 oxidation.

S6-M monolith shows the lowest H_2 consumption (Table 4), due to its low Cu content. Nevertheless, H_2/Cu ratio is in line with those observed for the other monoliths. The shape of the corresponding TPR profile suggests that more peaks could be identified on this sample, as reported for the other monoliths. However, fitting of the TPR profile does not provide consistent results.

3.5. Catalytic activity

In Fig. 9 CO conversion (a) and selectivity (b) are reported as a function of the maximum temperature measured inside the monolithic reactor for the different monoliths in absence of CO_2 and H_2O and at a fixed value of the contact time ($\tau = 0.054\ g_{cat}\ s/ml(STP)$).

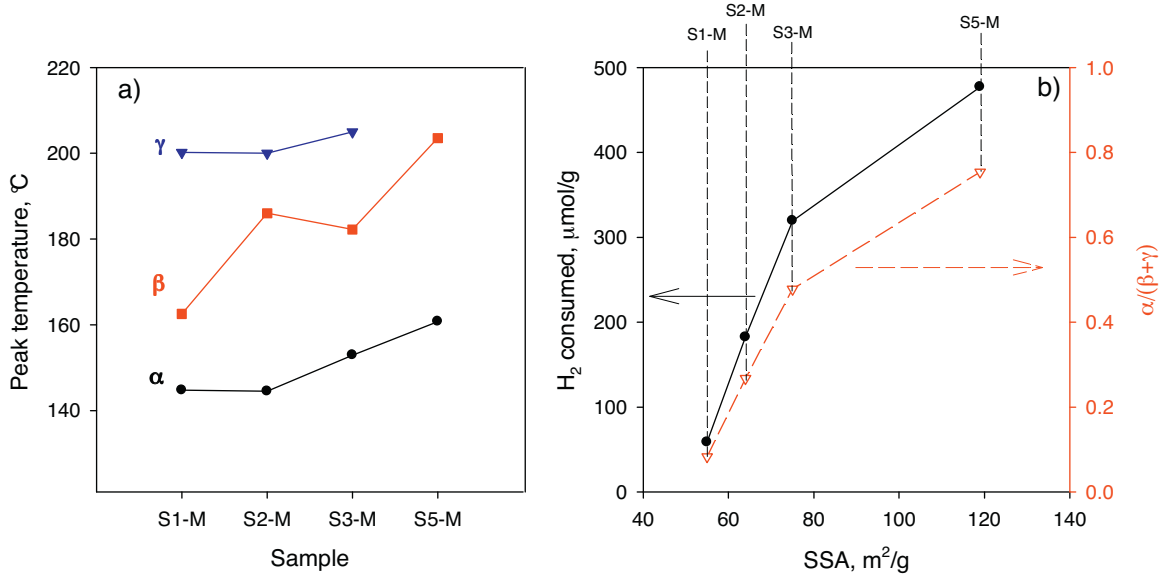

Fig. 8. Peak temperatures for different structured catalysts (a). H_2 consumed in the α peak (full symbols) and its ratio with H_2 consumed in the β and γ peaks (empty symbols) as a function of the SSA for structured CuO/CeO_2 catalysts (b).

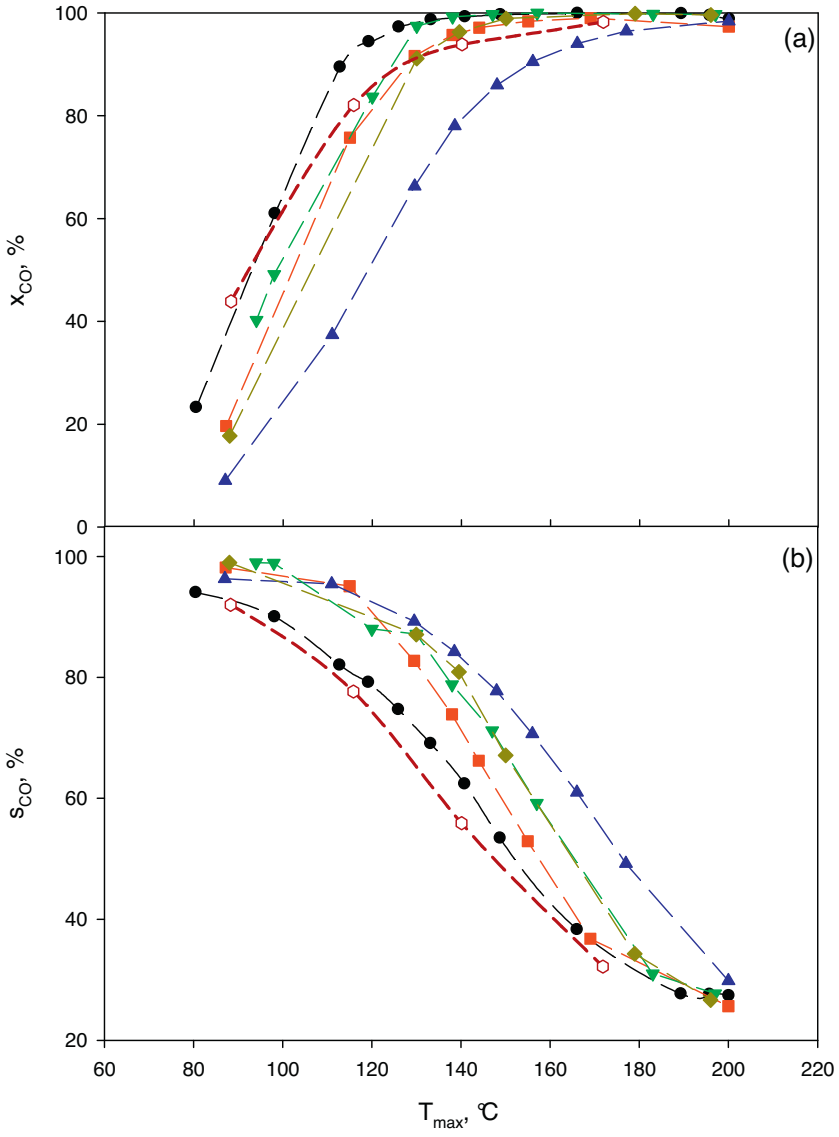

Fig. 9. CO conversion (a) and selectivity to CO_2 (b) as a function of the maximum temperature for different monoliths: S1-M (●); S2-M (■); S3-M (▼); S5-M (◆); S6-M (▲). Empty symbols refer to reference powder activity. $CO/O_2/H_2 = 0.5/0.9/50$. (For interpretation of the references to colour in this figure legend, the reader is referred to the web version of this article.)

In Fig. 10 the conversion-selectivity plot is also shown. In both graphs conversion and selectivity obtained on the powder sample are reported as reference.

S6-M monolith shows the lowest conversion in the whole range of temperature investigated; this behavior is related to its lower actual copper content, due to Cu leaching in the acid slurry, as reported in § 3.2. Selectivity to CO_2 obtained on this sample is, however, the highest. The selectivity values are certainly affected by the lower CO conversion; nevertheless, a selective leaching of copper sites active towards hydrogen oxidation cannot be excluded. Notwithstanding, the relationship between conversion and selectivity reported in Fig. 10 shows that this monolith is intrinsically less selective confirming the results of TPR analysis which demonstrated that big clusters of copper oxide are not selectively removed from the catalyst in the acid suspension but that also removal of CO oxidation sites occurs.

At low temperatures, all monoliths except S1-M show CO conversions lower than that obtained on the powder catalyst. This result can be explained by the partial occlusion on the catalyst due to ceria penetration into the cordierite macropores. This is in agreement with the higher temperatures required for CO oxidation sites found in the TPR experiments. At high temperatures, monoliths outperform due to the absence of intra-particle mass transfer control found in the powders [13]. From Fig. 9b we found that in the temperature range 110–130 °C, the order of selectivity to CO_2 is:

$$S1\text{-}M < S2\text{-}M < S3\text{-}M \leq S5\text{-}M$$

It is interesting to note that the scale of selectivity is in the same relationship of the scale of SSA and it is coherent with the H_2 TPR analysis and in particular with the α peak related sites thus confirming the relationship among selectivity and TPR analysis.

From the results of the monoliths characterizations we can conclude that the use of nanometric ceria for the washcoat of ceramic monolith improves adhesion and copper dispersion at the same time. Nevertheless, by comparing the catalytic performances of the monoliths in terms of conversion-selectivity relationship (Fig. 10) an unique order cannot be found. S3-M monolith outperforms. This is the result of the higher number of CO oxidation sites, related to the addition of ceria nanoparticles present in the colloidal sus-

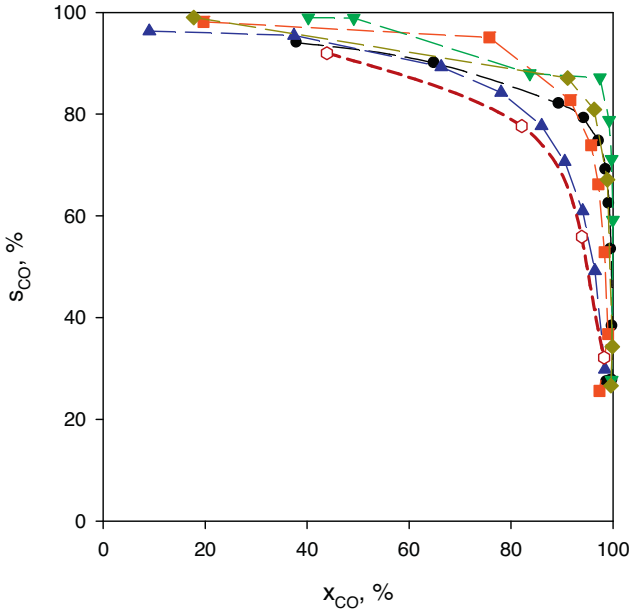

Fig. 10. Selectivity to CO_2 as a function of CO conversion for different monoliths: S1-M (●); S2-M (■); S3-M (▼); S5-M (◆); S6-M (▲). Empty symbols refer to the activity of the reference powder catalyst. $CO/O_2/H_2 = 0.5/0.9/50$. (For interpretation of the references to colour in this figure legend, the reader is referred to the web version of this article.)

pension, and the reduced penetration of the washcoat into the cordierite macropores, as evidenced by SEM images.

Finally, we checked the mechanical stability of monoliths under more severe flow conditions approaching those of real applications, thus verifying if the washcoat is eroded at higher linear velocities. Since the dimensions of the monolith are fixed, the test was performed on S3-M by increasing the Gas Hourly Space Velocity (GHSV) from about 27,000 h^{-1} (experiments reported in Fig. 8) to 45,000 h^{-1}; the test lasted 15 h and was carried out at 120 °C. Results (not reported) showed that catalytic performance was stable and the catalyst weight after this test was practically unchanged, thus confirming the good washcoat adhesion at high linear velocities too.

A direct comparison of the performance of our monoliths with those reported in the literature is not trivial, due to the different active phase used and reaction conditions adopted. Moreover, some works have been carried out on micro-reactors [7,8,11], showing a surface to volume ratio (and, thus, a catalyst weight to reactor volume ratio) significantly higher than monoliths; as a consequence, the GHSVs calculated on micro-reactors are higher than those obtained on monoliths even at the same catalyst load.

By looking at Fig. 9, we can assert that our best monoliths show about 100% CO conversion at maximum reactor temperatures higher than 130 °C with about 80% selectivity; calculated GHSV corresponds to 27,000 h^{-1}, O_2/CO ratio is equal to 1.8 and CO_2 and H_2O are absent in the feed. 400 cpsi cordierite [9,10,12] and FeCrAlloy [6] monoliths have been used with both CuO/CeO_2 [6,9] and Pt based [10,12] catalysts. Complete (or quite complete) CO conversion is generally obtained with GHSV between 9000 and 35,000 h^{-1} and at temperatures between 90 and 180 °C, depending on the active phase, inlet CO concentration and CO_2 and H_2O partial pressures. The catalysts showing the best performance on 400 cpsi monoliths, proposed by Farrauto and co-workers [10,12], contain high Pt loading (5 wt.% with respect to the active layer) and, as generally occurring on Pt-based systems, low selectivity. 400 cpsiCuO/CeO_2 monoliths were studied by Ayastuy et al. [9]; they found complete CO conversion at about 120 °C in the absence of CO_2 and H_2O in the feed with a GHSV equal to 9000 h^{-1}. Consequently, our monoliths outperform those reported in [9]. Goerke et al. [7] and Snytnikov et al. [11] deposed thin layer of CuO/CeO_2 catalyst onto stainless steel micro-channels. The GHSVs they used are generally higher than that reported in this work, but it is due to the peculiar features of micro-reactors, as reported above. High CO conversions are generally obtained at high temperature (>160 °C) and are coupled with low selectivity, due to the strong activation of hydrogen oxidation at those temperatures [18].

Even if the aim of this work is not the optimization of the reaction conditions of a CO-PROX monolithic reactor, we can conclude that the "non-optimized" performance of our monolithic reactors are in line, and in some cases better, with respect those reported in the literature on copper/ceria systems. Pt-based catalysts generally showed better performance, but are characterized by a high noble metal content.

4. Conclusions

In this work the effect of the slurry preparation on the washcoat adhesion and on the performances of structured CuO/CeO_2 monolithic catalysts towards CO-PROX reaction was studied.

CuO/CeO_2 monoliths were prepared by dip-coating procedure trying to improve washcoat adhesion over cordierite walls by changing the ceria particle size distribution. A larger fraction of ceria nanoparticles in the slurry was obtained by wet milling the starting ceria powder or by addition of colloidal ceria. These modifications of the preparation method assured a significant improvement of ceria adhesion with anegligible loss of washcoat due to the partial penetration of ceria washcoat into the cordierite macropores.

The presence of nanoparticle in the slurry modified some structural properties of the wahcoat, such as specific surface area and pore size distribution. The larger specific surface area was related to a better dispersion of copper, as suggested by a larger amount of CO oxidation sites titrated by H_2 TPR.

These good features prevail on the partial penetration of the active phase into the cordierite pores leading to lower performances at low temperature but providing conversion and selectivity higher than the reference powder catalyst at $T > 100$ °C.

Thus copper/ceria monolithic catalysts prepared according to the procedure proposed in this work can be good candidates for compact CO-PROX stage, especially in the case of non stationary applications.

Acknowledgement

This work was financially supported by Italian MIUR (FIRB2010 "Futuro in Ricerca", project no. RBFR10S4OW).

References

[1] D. Trimm, Z. Onsan, Onboard fuel conversion for hydrogen fuel-cell driven vehicles, Catal. Rev. Sci. Eng. 43 (2001) 31–84.
[2] I. López, T. Valdés-Solís, G. Marbán, An attempt to rank copper-based catalysts used in the CO-PROX reaction, Int. J. Hydrogen Energy 33 (1) (2008) 197–205.
[3] T. Giroux, S. Hwang, Y. Liu, W. Ruettinger, L. Shore, Monolithic structures as alternatives to particulate catalysts for the reforming of hydrocarbons for hydrogen generation, Appl. Catal. B Environ. 56 (2005) 95–110.
[4] C. Gu, S. Lu, J. Miao, Y. Liu, Y. Wang, Meso–macroporous monolithic $CuO–CeO_2/\gamma/\alpha$-Al_2O_3 catalysts for CO preferential oxidation in hydrogen-rich gas: effect of loading methods, Int. J. Hydrogen Energy 35 (2010) 6113–6122.
[5] F. Cipitì, L. Pino, A. Vita, M. Laganà, V. Recupero, Performance of a 5 kWe fuel processor for polymerelectrolyte fuel cells, Int. J. Hydrogen Energy 33 (2008) 3197–3203.
[6] S.H. Zeng, Y. Liu, Y.Q. Wang, $CuO–CeO_2/Al_2O_3$ /FeCrAl monolithic catalysts prepared by sol-pyrolysis method for preferential oxidation of carbon monoxide, Catal. Lett. 117 (3–4) (2007) 119–125.
[7] O. Goerke, P. Pfeifer, K. Schubert, Water gas shift reaction and selective oxidation of CO in microreactors, Appl. Catal. A Gen. 263 (2004) 11–18.

[8] G. Chen, Q. Yuan, H. Li, S. Li, CO selective oxidation in a microchannel reactor for PEM fuel cell, Chem. Eng. J. 101 (2004) 101–106.
[9] J.L. Ayastuy, N.K. Gamboa, M.P. González-Marcos, M.A. Gutiérrez-Ortiz, CuO/CeO_2 washcoated ceramic monoliths for CO-PROX reaction, Chem. Eng. J. 171 (2011) 224–231.
[10] Q. Zhang, L. Shore, R.J. Farrauto, Selective CO oxidation over a commercial PROX monolith catalyst for hydrogen fuel cell applications, Int. J. Hydrogen Energy 37 (14) (2012) 10874–10880.
[11] P.V. Snytnikov, D.I. Potemkin, E.V. Rebrov, V.A. Sobyanin, V. Hessel, J.C. Schouten, Design scale-out, and operation of a microchannel reactor with a Cu/CeO_{2-x} catalytic coating for preferential CO oxidation, Chem. Eng. J. 160 (2010) 923–929.
[12] O. Korotkikh, R. Farrauto, Selective catalytic oxidation of CO in H_2: fuel cell applications, Catal. Today 62 (2000) 249–254.
[13] P.S. Barbato, A. Di Benedetto, G. Landi, L. Lisi, CuO/CeO_2 based monoliths for CO preferential oxidation in H_2-rich streams, Chem. Eng. J. 279 (2015) 983–993, http://dx.doi.org/10.1016/j.cej.2015.05.079.
[14] A. Martínez-Arias, M. Fernández-Garcıía, O. Gálvez, J.M. Coronado, J.A. Anderson, J.C. Conesa, J. Soria, G. Munuera, Comparative study on redox properties and catalytic behavior for CO oxidation of CuO/CeO_2 and $CuO/ZrCeO_4$ catalysts, J. Catal. 195 (2000) 207–216.
[15] G. Sedmak, S. Hocevar, J. Levec, Kinetics of selective CO oxidation in excess of H_2 over the nanostructured $Cu_{0.1}Ce_{0.9}O_{2-y}$ catalyst, J.Catal. 213 (2003) 135–150.
[16] J.B. Wang, W.-H. Shih, T.-J. Huang, Study of Sm_2O_3-doped CeO_2/Al_2O_3-supported copper catalyst for CO oxidation, Appl.Catal. A Gen. 203 (2) (2000) 191–199.
[17] T. Caputo, R. Pirone, G. Russo, Supported $CuO/Ce_{1-x}Zr_xO_2$ catalysts for the preferential oxidation of CO in H_2-rich gases, Kinet. Catal. 47 (5) (2006) 756–764.
[18] T. Caputo, L. Lisi, R. Pirone, G. Russo, Kinetics of the preferential oxidation of CO over CuO/CeO_2 catalysts in H_2-rich gases, Ind. Eng. Chem. Res. 46 (21) (2007) 6793–6800.
[19] M. Monte, D. Gamarra, A. LópezCámara, S.B. Rasmussen, N. Gyorffy, Z. Schay, A. Martínez-Arias, J.C. Conesa, Preferential oxidation of CO in excess H_2 over CuO/CeO_2 catalysts: Performance as a function of the copper coverage and exposed face present in the CeO_2 support, Catal. Today 229 (2014) 104–113.
[20] A. Martínez-Arias, A.B. Hungría, M. Fernández-García, J.C. Conesa, G. Munuera, Preferential oxidation of CO in a H_2-rich stream over CuO/CeO_2 and $CuO/(Ce,M)\ O_x$ (M = Zr, Tb) catalysts, J. Power Sources 151 (1-2) (2005) 32–42.
[21] A. Martínez-Arias, A.B. Hungría, G. Munuera, D. Gamarra, Preferential oxidation of CO in rich H_2 over CuO/CeO_2: details of selectivity and deactivation under the reactant stream, Appl. Catal. B Environ. 65 (3–4) (2006) 207–216.
[22] S. Lang, M. Türk, B. Kraushaar-Czarnetzki, Novel $PtCuO/CeO_2/\alpha$-Al_2O_3 sponge catalysts for the preferential oxidation of CO (PROX) prepared by means of supercritical fluid reactive deposition (SFRD), J. Catal. 286 (2012) 78–87.
[23] M. Wojdyr, Fityk: a general-purpose peak fitting program, J. Appl. Cryst. 43 (1126) (2010).
[24] A. Di Benedetto, G. Landi, L. Lisi, G. Russo, Role of CO_2 on CO preferential oxidation over CuO/CeO_2 catalyst, Appl. Catal. B Environ. 142–143 (142) (2013) 169–177.
[25] A.V. Neimark, Y. Lin, P.I. Ravikovitch, M. Thommes, Quenched solid density functional theory and pore size analysis of micro-mesoporous carbons, Carbon 47 (2009) 1617–1628.
[26] C. Agrafiotis, A. Tsetsekou, C.J. Stournaras, A. Julbe, L. Dalmazio, C. Guizard, Evaluation of sol-gel methods for the synthesis of doped-ceria environmental catalysis systems. Part I: preparation of coatings, J. Eur. Ceram. Soc. 22 (2002) 15–25.
[27] D. Tsogtkhangai, S.V. Mamyachenkov, O.S. Ansimova, S.S. Naboichenzo, Kinetics of leaching of copper concentrates by nitric acid, Russian Journal of Non-Ferrous Metals 52 (2011) 469–472.
[28] T. Caputo, L. Lisi, R. Pirone, G. Russo, On the role of redox properties of CuO/CeO_2 catalysts in the preferential oxidation of CO in H_2-rich gases, Appl. Catal. A Gen. 348 (2008) 42–53.
[29] G. Fierro, M. Lo Jacono, M. Inversi, P. Porta, R. Lavecchia, F. Cioci, A Study of Anomalous Temperature-Programmed Reduction Profiles of Cu_2O, CuO, and CuO-ZnO Catalysts, J. Catal. 148 (1994) 709.
[30] A. Martinez-Arias, D. Gamarra, M. Fernandez-Garcia, A. Hornes, P. Bera, Zs. Koppany, Z. Schay, Redox-catalytic correlations in oxidised copper-ceria CO-PROX catalysts, Catal. Today 143 (2009) 211–217.
[31] M.F. Luo, Y.J. Zhong, X.X. Yuan, X.M. Zheng, TPR and TPD studies of CuO/CeO_2 catalysts for low temperature CO oxidation, Appl. Catal. A Gen. 162 (1997) 121–131.